

Tanya M. Brown

*Insurance Institute for Business & Home Safety*

Ian M. Giammanco

*Insurance Institute for Business & Home Safety*

Matthew R. Kumjian

*The Pennsylvania State University*

## 1. INTRODUCTION

Severe hail events are responsible for nearly \$1 billion in annual insured property losses in the United States (Changnon *et al.* 2009). Despite a general negative trend in population growth across the Great Plains of the United States, an increasing trend in hail-related losses has been observed over the past decade (MunichRe 2013). An increase in property damage has been documented (Smith *et al.* 2012) despite a decreasing trend in number of hail days per year (Changnon *et al.* 2009). With increasing property losses, there is a renewed interest in understanding how the characteristics and material properties of hail may influence damage associated with the existing building stock and new construction.

Characteristics of hailstones, such as size, mass, embryo type, and growth processes have been well documented in historical literature (Browning 1963; Browning and Foote 1976; Browning 1977; Macklin 1977; Foote and Knight 1977; Zeigler *et al.* 1983; Knight and Knight 2001). It is often assumed that damage states will scale perfectly with impact kinetic energy, which is reflected in standardized material impact test methodologies utilizing a steel ball (UL 2218) or pure ice sphere (FM 4473) to represent a hailstone. The methods match the theoretical impact kinetic energy of projectiles to that which similarly-sized hailstones would have when falling at theoretical terminal velocities (assuming no wind, fixed drag coefficient, spherical shape, and hailstone

density equal to that of pure ice at  $0.9 \text{ g cm}^{-3}$ ), based on the work of Laurie (1960).

However, post-event surveys and closed claims studies have shown discrepancies between building product performance and laboratory test ratings. Little is known about the material properties of natural hail (Kim and Kedward 2000; Schulson and Duval 2009; Swift 2013). Historical studies often qualitatively describe hailstones as: “hard”, “soft” or “slushy” with no quantitative means to describe them (Bilhelm and Relf, 1937; Carte 1966; Knight and Knight 1973). It is hypothesized that in addition to kinetic energy, the hardness property of individual hailstones may also affect resulting building damage, as influenced by the material properties of the hailstone and those of the object it impacts. Knight *et al.* (2008) speculated that little property damage was likely associated with an observed hail event which produced “soft” hailstones of sizes larger than 4 cm, which is much larger than the 2.54 cm severe hail criteria.

In 2012, the Insurance Institute for Business & Home Safety (IBHS) began a comprehensive research program focused on understanding the damaging potential of hail (Brown *et al.* 2012; Giammanco and Brown 2014). In addition to laboratory work, field teams collect research grade, in-situ measurements of the characteristics of hail (e.g. dimensions, mass, peak compressive force at fracture, photographic catalog) from Great Plains storms. Beginning in 2014, teams also explored ways to collect time histories of hail impact energies and size distributions using rapidly-deployable hail impact disdrometers.

In addition to building a database of hail characteristics, the field phase of the research

---

\*Corresponding Author Address: Tanya M. Brown, PhD. Insurance Institute for Business & Home Safety Research Center, 5335 Richburg Rd, Richburg SC 29729. [tbrown@ibhs.org](mailto:tbrown@ibhs.org)

program seeks to understand how the synoptic and mesoscale environments and convective mode may affect the type of hailstone produced (e.g. soft, hard, slushy). The environmental conditions conducive for hail production are well documented (List 1985; Rogers and Yau 1989; Thompson *et al.* 2012). Examining conditions which yield a harder type of hailstone may help assess which conditions may lead to more damaging hail events. Additionally, with the nationwide upgrade of the WSR-88D network to dual-polarization technology in 2013, ground-based cross-swath hail data have proven useful in providing validation data for improving radar-based hail detection algorithms.

The 2012-2014 field phases have yielded a dataset of 2557 hailstones from 33 parent thunderstorms. Figure 1 provides a map of all data collection locations.

## 2. OBJECTIVES

The field phase of the research program has evolved over a three-year period, as capabilities, technology, and resources have changed. The number of objectives has increased as logistics, experimental plans, and measurement processes have improved. The primary objectives are summarized as follows:

1. Obtain quality spatial resolution hail measurements in the cross-swath axis;
2. Collect representative hail size distributions for each measurement location;
3. Photographically document the distribution of hail at each measurement location;
4. Provide validation data for laboratory impact testing of building materials;
5. Provide ground-truth validation data for developing radar-based hail detection algorithms; and
6. Provide ground-truth validation data for modeling applications.

In 2014, additional objectives included:

1. Effectively measure three dimensions of hailstones;
2. Obtain compressive stress measurements of large hail (> 1 in.);

3. Collect pilot hail impact disdrometer data;
4. Evaluate measurement differences between two hail impact disdrometer prototypes; and
5. Examine the feasibility of hail impact disdrometers to function as an adaptive deployable observing network or fixed platform sensor.

## 3. EXPERIMENTAL PLAN

Teams operated in the Great Plains region of the United States, where good visibility and quality gridded road networks allow for safe intercepts of severe thunderstorms. This region generally experiences more severe hail events than other parts of the U.S. (Changnon *et al.*, 2009). Forecast preference was given to regions with the necessary conditions for supercell thunderstorms since this type of thunderstorm exhibits the highest probability for significant hail (Browning 1963; Browning 1977; Lemon and Doswell 1979; Doswell and Burgess 1993). To maximize opportunities for data collection, teams were nomadic, following the methodology of VORTEX II (Wurman *et al.* 2012) and others. Target operations regions were selected daily. Target storms were selected based on their radar presentation and the ambient environment in which they were embedded.

Once a target storm was selected, measurement teams positioned themselves in close proximity to the storm, while remaining safe and outside the region of hailfall. Teams assigned to deploy hail impact disdrometers proceeded into the forecasted path of the storm and deployed instruments, before retreating to a safe position. The two hail impact disdrometers were generally collocated for sensitivity comparisons. Thus, the margin for error was quite small given the lead time required to safely deploy them.

Field measurement teams were responsible for collecting stones immediately following passage of the thunderstorm targeted for data collection. Safety considerations necessitated a time lag between the time stones reached the ground and when they were collected. In some instances this lag was as long as 30–40 minutes. When safe, teams drove toward the anticipated region of hail based on radar presentation, and checked for the

presence of hail. One team began measurements at the first location where hail was present, while other teams moved further into the hail swath. Measurement locations were generally spaced 0.4-1.6 km apart, and were dependent upon the estimated spatial extent of the swath. Measurements were always made at the location of the hail impact disdrometers. Efforts were made to measure stones at points across the entire swath, but the proximity of nearby storms occasionally required teams to retreat to maintain safe positions.

#### **4. MEASUREMENTS AND DATA COLLECTION**

Visual observations of hailstones on the ground indicated that hailstones could efficiently insulate themselves, especially when large quantities were present. Hail could also persist in grassy areas for some time after the parent thunderstorm had passed. Nevertheless, the unavoidable time lag between when hail fell and when teams arrived to begin measurements introduced a source of error due to melting. It is accepted that some mass and diameter loss occurred prior to collection. Sharp protuberances were likely rounded due to melting; also, liquid water may have filled existing voids within the stone, thus introducing a positive bias in the measured mass.

In an effort to collect a robust hail dataset, each hailstone was photographically cataloged, an example of which is provided in Figure 2. Dimensions of each stone were measured assuming that two dimensions of the stone ( $x_1 \approx x_2$ ) are relatively similar and larger than the third ( $y$ ). A reasonable estimate of the cross-sectional area of the hailstone could be determined. In 2014, measurement of the third dimension of each stone was added for some cases. The photograph of each stone coupled with its physical measurements allowed shape to be effectively classified, as shown in the companion paper (Giammanco *et al.* 2014). Each stone was also weighed. Data were input and recorded via a National Instruments LabVIEW user interface, which also recorded GPS position and time.

A rugged and portable piece of instrumentation was developed that utilizes a load cell to measure the compressive force of hailstones at fracture (Brown *et al.* 2012). The compressive force is

used to calculate the compressive stress required to fracture the stone as a way to evaluate the hardness property. The rate of force applied to the stone is large enough to produce a brittle failure of the stone. At slow rates of deformation, ice typically exhibits a more ductile failure (Schulson 1997). The same LabVIEW script used to input diameter and mass data is used as a data acquisition interface to measure the compressive force applied to hailstones (Brown *et al.* 2012). It should be noted however, that the compressive force test methodology exhibits a low bias when compared to tests conducted with a Universal Testing Machine (UTM), due to sampling limitations. This is being researched.

In 2014, two rugged and rapidly-deployable prototype hail impact disdrometer probes, shown in Figure 3, were developed to capture time histories of hail size distributions and impact energies. The probes follow the design of Lane *et al.* (2006). The probes use one (“A” type probe) or multiple (“B” type probe) piezo-electric disks to sense the impact of falling hail and/or rain (Mikhaylovskaya 1964; Joss and Waldvogel 1967; Kinnell 1972). Through empirical relationships, the size distribution of falling hail can be extracted from the sensor signals. The probes have an integrated GPS module for position and time synchronization. Additional development is needed to process raw sensor information into meaningful near real-time hail impact concentrations. Field measurements of hail at probe deployment sites, coupled with laboratory impact testing will allow hail size discrimination algorithms to be developed. While similar sensors are commercially available, they are generally cost prohibitive, not rapidly-deployable in a research setting, and not rugged enough to withstand repeated exposure to large hail.

#### **5. HAILSTONE DATABASE**

The 2012-2014 dataset contains 2557 hailstones measured during 14 operation days, from 33 parent thunderstorms. Table 1 provides a summary of each sampled thunderstorm and the associated hail distribution. The sizes of hailstones measured ranged from as small as 0.11 cm to as large as 10.7 cm. The mean measured hailstone dimension was 1.81 cm.

The mean mass of the measured hailstones was 4.72 g with 90% of the dataset falling below 12 g. The most massive stone measured was 163.3 g which was associated with the largest diameter measured. This stone was found near Ratliff City, OK on 30 May 2013. The mass-diameter relationship with a fitted power law curve for the field data is shown in Figure 4, along with the relationship for pure ice spheres for the range of densities observed in historical literature.

Compressive stress was used to represent the hardness property of measured hailstones. Compressive stress values ranged from stones which were too slushy to test to a maximum of 55.15 mPa. The mean value of the compressive stress distribution was 0.88 mPa. The probability distribution is shown in Figure 5, with a fitted Gamma distribution. The largest compressive stress values were typically not associated with the largest diameter hailstones. Haynes (1978) found a mean compressive stress of ice structures of 1.43 mPa at temperatures of -10 to -20 C, which is about 60% higher than the mean measured in this study. The field phase compressive stress data have a large range of values, and data were collected at much warmer temperatures (10 to 30 C). The use of cross-sectional area may lead to small errors in the calculated compressive force, as stones may not fracture exactly along this plane. Approximately 16% of the cataloged stones were not tested for compressive force. These were either too spongy; exhibited a ductile failure such that a peak compressive force could not be effectively determined; or the team leader elected not to perform the test to increase the number of stones for which mass and diameter were measured.

Three quality datasets were obtained from the hail impact disdrometers. Hailstones approaching the 2.54 cm severe criteria were measured at each deployment site. The deployment on 5 June 2014 was one of the most successful as both probes were deployed into a thunderstorm near Punkin Center, Colorado that produced a large volume of small hail with two distinct pulses in hailfall. The processed data from both probes is shown in Figure 6 as impacts per minute, the magnitude of which are presented as percentage of the full-scale range of the instrument, grouped into magnitude bins. Size and kinetic energy

relationships to translate these bins into hail characteristics will be developed.

Two distinct periods of small hail with relatively large concentrations (~10-20 impacts per minute) were evident. However, there are differences in the representation between the two probes. Each probe resolved the relative lull in hailfall between 23:20 and 23:26 UTC which is well correlated with radar trends. Probe 0101A indicated a high impact concentration beginning at 23:22 UTC through the end of the record in the lowest magnitude group. It is believed the probe was actually resolving a high concentration of large rain drops in the lowest magnitude group (> 80 impacts per minute). It is unclear where exactly the threshold between large rain drops and hail lies, but further sensitivity testing in strictly rainfall environments and in the laboratory will help to identify this.

The impact probes were effective in capturing the fine-scale structure within the hail swath. Radar data indicated the storm was evolving quickly as it passed over the probe locations with several pulses in intensity, which were well-captured by the two distinct peaks and local minima in hailfall observed by the probes. It is likely this particular storm did not produce a continuous swath of hail but sporadic "streaks" which were described by Changnon (1970).

## 6. LABORATORY COMPARISONS

To compare field observations to projectiles used in standard impact tests, ice spheres of tap and distilled water (FM 4473) were made using spherical molds of 3.175 cm (1.25 in.), 4.445 cm (1.75 in), and 5.715 cm (2.25 in.). The molds were placed in a freezer at approximately -20 C for 24 hours. Laboratory stones were measured, weighed, and tested for compressive force in the same fashion as those collected in the field.

The mass-diameter relationship was examined for the two datasets. The results are shown in Figure 7. The tap and distilled water stones fit very closely to a spherical volume equation with a density of 0.9 g cm<sup>-3</sup> as shown in the companion paper (Giammanco *et al.* 2014), while the field hailstones are biased towards a lower mass. There are two primary causes: 1) the use of purely spherical and thus more massive

laboratory stones; 2) the higher density of pure ice spheres (approximately  $0.9 \text{ g cm}^{-3}$ ) compared to lower ranges documented in historical literature ( $0.2$  to  $0.9 \text{ g cm}^{-3}$ ). Laboratory ice spheres were predominately clear ice with small trapped bubbles and very small expansion cracks. The photographs of natural hail revealed a larger percentage of trapped bubbles and classic layered structure as a result of alternating growth processes (Knight and Knight 2001). Additional solutions using dissolved  $\text{CO}_2$  to produce a larger percentage of trapped bubbles and spheres comprised of compacted crushed ice have been investigated. The presence of expansion cracks in laboratory spheres led to large variability in the compressive stress measurements as stones often cracked along pre-existing fractures. Additional work is needed to refine laboratory processes to produce a more consistent stone. Although natural hailstone are subject to expansion cracks, for laboratory test applications a more consistent and reproducible stone is desired.

Compressive stresses were plotted for binned groups of the individual laboratory datasets and the field dataset. Results are shown in Figure 8. Field data were binned by equivalent diameter using  $0.635 \text{ cm}$  ( $0.25 \text{ in.}$ ) bin sizes for comparison with the three sizes of laboratory ice spheres. It is readily apparent the mean compressive stresses of the field data are similar to tap and distilled water ice spheres produced in a laboratory setting. These stones represent a reasonable approximation of the mean compressive stress of natural hailstones observed in the Great Plains region during the 2012-2014 field campaign.

## **7. SUMMARY**

The data collected during the 2012-2014 IBHS field phases has provided a much needed baseline to evaluate the representativeness of existing laboratory impact test methodologies. The compressive force test applied to natural hailstones has also provided a quantitative means to describe the hardness property of a given stone.

The overall sample size from the three years of field measurement is miniscule compared to the number of stones a single thunderstorm can produce, but the database is believed to be the

largest research-quality database of hailstones in existence.

The typical dimension of stone measured during the three year field phase was approximately  $1.8 \text{ cm}$  with 63% of the measurements falling below the severe threshold ( $2.54 \text{ cm} / 1 \text{ in.}$ ). Mean compressive stresses measured in the field were generally similar to those found in laboratory testing of clear ice using the same instrument. However, the field data exhibited a much larger range of values.

The experience gained from the prototype hail impact disdrometers will guide the development of an adaptive deployable network of probes. A pilot network of fixed probes will be installed on existing surface weather observing stations in hail-prone regions of West Texas beginning in 2015. As development continues, the platforms will be able to provide an estimate of hail concentration by volume. This will allow for hail size distributions to be created and compared with historical and theoretical hail size distributions. The probes also offer additional ground-truth observations of hail for comparison with polarimetric radar hail detection products. For engineering applications, these data will allow for accurate full-scale event simulations.

Comparisons between laboratory and natural hailstones yielded interesting results. The relationship between mass and diameter suggests that the kinetic energy of laboratory stones is higher than stones of a similar maximum diameter observed in the field. This is a result of the varying shapes observed in the field and their associated mass-diameter curves versus pure ice spheres used in laboratory testing. For material impact tests, the use of propulsion speeds derived from terminal velocity estimates assuming a perfect sphere would yield a higher kinetic energy than a natural stone falling at the same velocity. When accounting for changes in drag resulting from non-spherical hailstone shapes and their non-homogeneous surfaces this difference may grow larger. It is intuitive that larger, more massive stones will produce more damage through increased kinetic energy. It is also understood that standardized laboratory test methodologies for hail impacts such as UL 2218 (2012) and FM 4473 (2005) are not perfectly representative of natural hail

impacts. In-situ damage observations and laboratory damage experiments coupled with observations of natural hail characteristics suggest ice spheres used in the FM 4473 method are adequate for representing the average hardness of a natural hailstone but are likely even more conservative with regards to impact kinetic energies. The contribution of the hardness property of hailstones and how it relates to the imparted force, duration of impact, and damage is not well understood. Future work will continue to focus on understanding this contribution and how common building materials perform in their new and aged states.

## 8. REFERENCES

- Bilhelm, E.G., and E.F. Relf, 1937: The dynamics of large hailstones. *Quart. J. Roy. Meteor. Soc.*, **63**, 149-162.
- Brown, T.M., I.M. Giammanco, and D.S. Robinett, 2012: Observations of hailstone characteristics utilizing a new instrumentation platform. *26<sup>th</sup> Conference on Severe Local Storms*, Nashville, TN.
- Browning, K.A., 1963: The growth of large hail within a steady updraught. *Quart. J. Roy. Meteor. Soc.*, **89**, 490-506.
- Browning, K.A., 1977: The structure and mechanisms of hailstorms: *A review of hail science and suppression*, *Meteor. Monogr.*, No. 38, Amer. Meteor. Soc., 1-43.
- Browning, K.A. and G.B. Foote, 1976: Airflow and hail growth in supercell storms and some implications for hail suppression. *Quart. J. Roy. Meteor. Soc.*, **102**, 499-533.
- Carte, A.E., 1966: Features of Transvaal hailstones. *Quart. J. Roy. Meteor. Soc.*, **92**, 290-296.
- Changnon, S.A., 1970: Hailstreaks. *J. Atmos. Sci.*, **27**, 109-125.
- Changnon, S.A., D. Changnon, and S.D. Hilberg, 2009: Hailstorms across the nation: An atlas about hail and its damages. Illinois State Water Survey Contract Report 2009-12, 78 pp.
- Doswell III, C.A. and D.W. Burgess, 1993: Tornadoes and tornadic storms: A review of conceptual models. *The Tornado: Its Structure, Dynamics, Prediction, and Hazards*, *Geophys. Monogr.*, No. 79, Amer. Geophys. Union, 161-172.
- FM Approvals. (2005). Specification test standard for impact resistance testing of rigid roofing materials by impacting with freezer ice balls (FM 4473). West Glocester, RI: FM Approvals.
- Foote, G.B., and C.A. Knight Eds., 1977: *Hail: A Review of Hail Science and Suppression*. Meteor. Monogr. No. 38, Amer. Meteor. Soc., 277 pp.
- Giammanco, I.M., and T.M. Brown, 2014: Observations Hailstone Characteristics in Multicell and Supercell Thunderstorms. *94<sup>th</sup> AMS Annual Meeting*, Atlanta, GA.
- Giammanco, I.M., T.M. Brown, M.R. Kumjian, A.J. Heymsfield, 2014: Observations of Hailstone Sizes and Shapes from the IBHS Hail Measurement Program. *27<sup>th</sup> Conference on Severe Local Storms*, Madison, WI.
- Haynes, F.D., 1978: Effect of temperature on the strength of snow-ice. Department of the Army, Cold Regions Research and Engineering Laboratory, Corps of Engineers, CRREL Report 78-27: Hanover, New Hampshire.
- Joss, J. and A. Waldvogel, 1967: Ein Spektrograph für Niederschlagstropfen mit automatischer Auswertung. *P. Appl. Geophys.*, **68**, 240-246.
- Kim, H., and K.T. Kedward, 2000: Modeling hail ice impacts and predicting impact damage initiation in composite structures. *AIAA Journal*, **38**, 1278-1288.
- Kinnell, P.I.A., 1972: The acoustic measurement of water-drop impacts. *J. Appl. Meteor.*, **11**, 691-694.
- Knight, C.A., and N.C. Knight, 1973: Quenched, spongy hail. *J. Atmos. Sci.*, **30**, 1665-1671.
- Knight, C.A. and N.C. Knight, 2001: Hailstorms in severe convective storms, Ed. Doswell C.A., *Amer. Meteor. Soc.*, Monograph, 223-254.
- Knight, C.A., P.T. Schlatter, and T.W. Schlatter, 2008: An unusual hailstorm on 24 June 2006 in

Boulder, Colorado. Part II: Low-density growth of hail. *Mon. Wea. Rev.*, **136**, 2833-2848.

Laurie, J.A.P., 1960: Hail and its effects on buildings. Council for Scientific and Industrial Research, Report No. 176, Pretoria, South Africa, 12 pp.

Lemon, L.R., and C.A. Doswell III, 1979: Severe thunderstorm evolution and mesocyclone structure as related to tornadogenesis. *Mon. Wea. Rev.*, **107**, 1184-1197.

List, R., 1985: Properties and growth of hailstones. *Thunderstorm morphology and dynamics*, E. Kessler Ed., University of Oklahoma Press, 259-276.

Macklin, W.C., 1977: The characteristics of natural hailstones and their suppression. *Hail: A Review of Hail Science and Suppression*, Meteor. Monogr., No. 38, Amer. Meteor. Soc., 65-88.

Mikhaylovskaya, V.V., 1964: Theory of measuring the size of raindrops by acoustic method. *Sov. Hydrol. Selected Papers*, **1**, 85-90.

MunichRe, 2013: *Severe Weather in North America: Perils, Risks, and Hazards*. P. Roeder, ed. 274 pp.

Rogers, R.R., and M.K. Yau, 1989: *A Short Course in Cloud Physics*. 3d ed Elsevier, 290 pp.

Schulson, E.M., 1997: The brittle failure of ice under compression. *J. Phys. Chem. B*, **101**, 6254-6258.

Schulson, E.M., and P. Duval, 2009: *Creep and Fracture of Ice*. Cambridge University Press. 416 pp.

Swift, J.M., 2013: Simulated hail ice mechanical properties and failure mechanisms at quasi-static strain rates. M.S. thesis, Department of Aeronautics and Astronautics, University of Washington, 71 pp.

Thompson, R.L., B.T. Smith, J.S. Grams, A.R. Dean, and C. Broyles, 2012: Convective modes for significant severe thunderstorms in the contiguous United States. Part II: Supercell and QLCS tornado environments. *Wea. Forecasting*, **27**, 1136-1154.

Smith, B.T., R.L. Thompson, J.S. Grams, and C. Broyles, 2012: Convective modes for significant severe thunderstorms in the contiguous United States. Part I: Storm classification and climatology. *Wea. Forecasting*, **27**, 1114-1135.

Underwriters Laboratory, 2012: *UL 2218: Standard for impact resistance of prepared roof covering materials*. Northbrook, IL: UL.

Wurman, J., D. Dowell, Y. Richardson, P. Markowski, E. Rasmussen, D. Burgess, L. Wicker, H.B. Bluestein, 2012: The second Verification of the Origins of Rotation in Tornadoes Experiment: VORTEX2. *Bull. Amer. Meteor. Soc.*, **93**, 1147-1170.

Ziegler, C.L., P.S. Ray, and N.C. Knight, 1983: Hail growth in an Oklahoma multicell storm. *J. Atmos. Sci.*, **40**, 1768-1791.

Table 1. Summary statistics for each thunderstorm event during the 2012-2013 field phase.

Case	Date	Location	Sample Size	Max Diameter (cm)	Mean Diameter (cm)	Max Compressive Stress (mPa)	Mean Compressive Stress (mPa)
1A-2012	5-27-12	Ravenna, NE	5	1.93	1.35	1.33	0.88
2A-2012	5-28-12	Lindsay, OK	32	4.75	2.77	2.21	0.89
3A-2012	5-29-12	Kingfisher, OK	20	7.75	2.31	3.71	1.24
3B-2012	5-29-12	Greenfield, OK	17	3.05	1.93	4.32	1.31
4A-2012	6-1-12	Channing, TX	45	3.12	1.80	4.20	0.85
5A-2012	6-2-12	Eads, CO	17	3.33	1.63	0.76	0.39
*6A-2012	6-6-12	Cheyenne, WY	36	3.23	1.44	0.54	0.22
7A-2012	6-7-12	LaGrange, WY	8	3.76	3.12	0.64	0.38
*7B-2012	6-7-12	LaGrange, WY	59	5.41	3.02	2.77	0.57
*1A-2013	5-17-13	Hyannis, NE	85	3.30	1.41	4.57	0.81
2A-2013	5-18-13	Paradise, KS	6	1.82	0.96	0.41	0.40
*3A-2013	5-19-13	Wichita, KS	112	3.20	1.47	4.24	0.61
3B-2013	5-19-13	Arkansas City, KS	16	3.43	1.51	1.51	0.64
*3C-2013	5-19-13	Blackwell/Newkirk, OK	23	2.51	1.11	1.51	0.55
*3D-2013	5-19-13	Cedar Vale, OK	71	3.99	2.08	1.12	0.29
3E-2013	5-19-13	Burbank, OK	18	2.21	1.11	1.80	0.95
*4A-2013	5-20-13	Antioch, OK	212	4.80	0.81	3.34	0.56
5A-2013	5-30-13	Blanchard, OK	15	3.98	2.08	1.58	0.59
*5B-2013	5-30-13	Ratliff City, OK	29	10.69	2.61	3.88	0.70
6A-2013	6-1-13	Mason, TX	29	2.99	1.60	7.46	1.64
6B-2013	6-1-13	London, TX	30	3.60	1.88	6.46	1.43
7A-2013	6-2-13	Elmwood, OK	36	3.71	1.88	2.86	0.51
1A-2014	5-7-14	Holiday, TX	6	2.90	2.03	8.56	n/a
*1B-2014	5-7-14	Lakeside City, TX	54	2.29	1.42	2.63	1.10
*1C-2014	5-7-14	Waurika, OK	239	5.72	2.64	n/a	n/a
*2A-2014	5-10-14	Latham, KS	71	2.29	1.30	2.88	0.66
*^2B-2014	5-10-14	Beaumont, KS	279	2.39	1.91	4.84	0.74
*^3A-2014	5-11-14	Greensburg, KS	113	2.41	1.40	3.17	0.97
*3B-2014	5-11-14	Larned, KS	46	2.62	1.80	1.67	0.88
*4A-2014	6-3-14	Oconto, NE	95	3.43	1.70	17.58	2.82
*4B-2014	6-3-14	Broken Bow, NE	228	6.76	2.57	20.39	1.19
*5A-2014	6-4-14	Hay Springs, NE	273	2.90	1.55	17.28	1.01
*^6A-2014	6-5-14	Punkin Center, CO	125	2.57	1.35	13.64	0.89
*7A-2014	6-6-14	Lakin, KS	107	3.76	2.16	1.17	0.54

\* multiple measurement locations within the swath of hailfall from the same parent updraft

^ associated hail impact disdrometer deployment

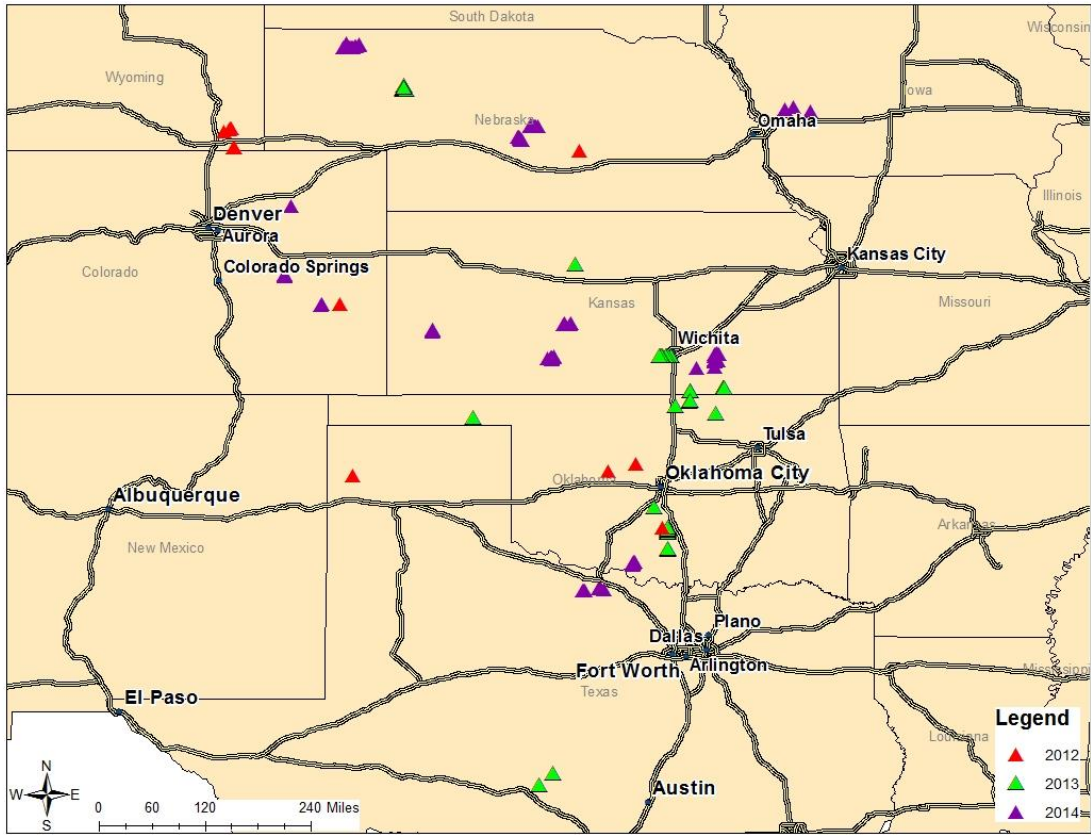


Figure 1. Map of all measurement locations during the 2012-2014 field phases.



Figure 2. Example of a hailstone catalog photograph.



Figure 3. Photograph of the two prototype hail impact disdrometers (A-type left, B-type right), deployed during the 2014 field phase.

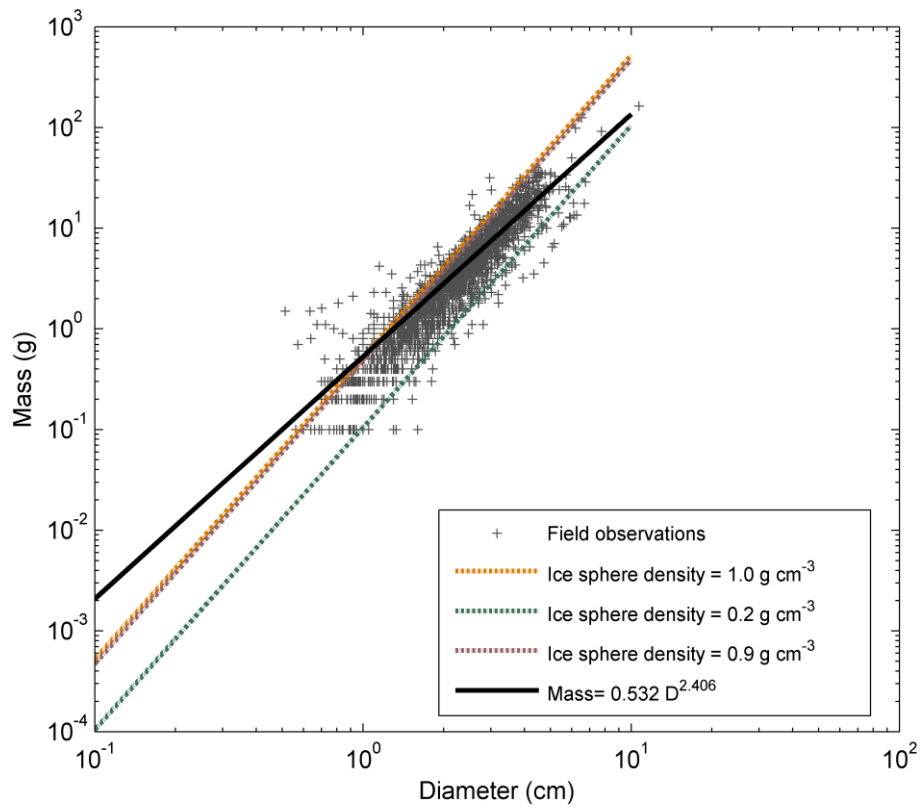


Figure 4. Hailstone mass as a function of major diameter and the power-law fitted curve for IBHS field measurements. Also shown are the pure ice sphere theoretical relationships for the range of historical hailstone density values.

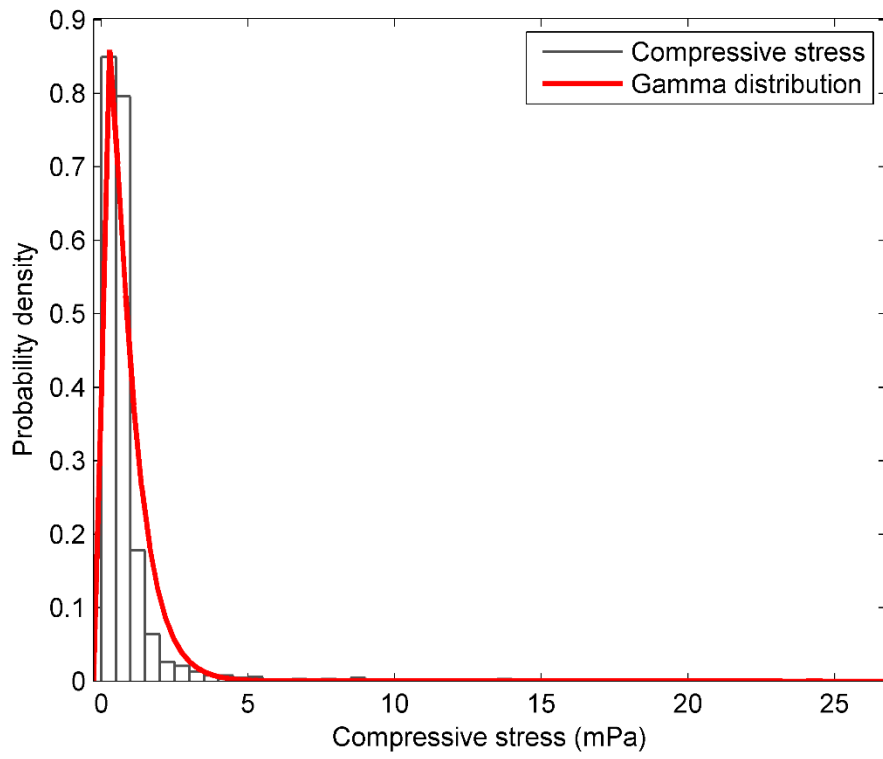


Figure 5. Hailstone compressive stress distribution for 2012-2014 field observations, with Gamma distribution fitted.

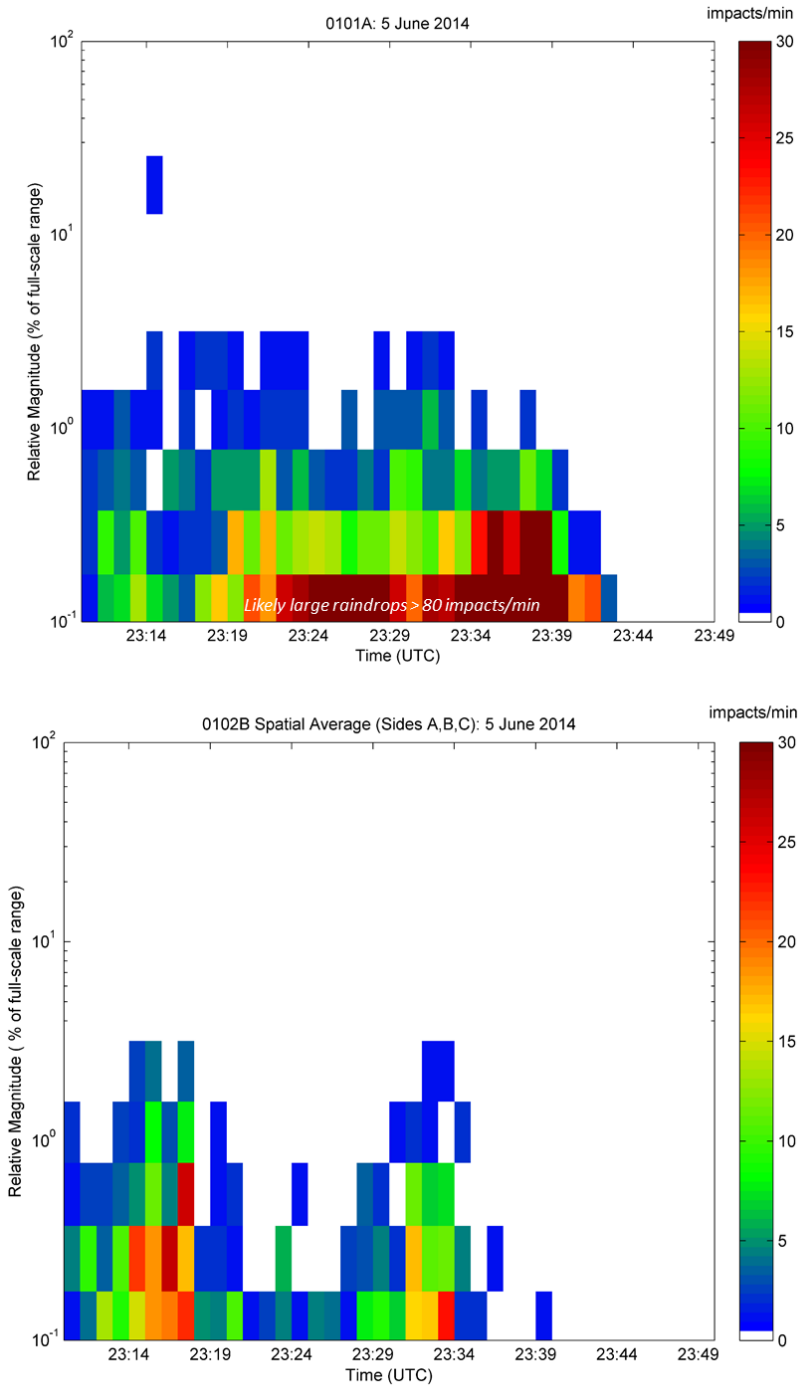


Figure 6. Impact concentrations per minute observed by hail impact disdrometer probe 0101A (top) and 0102B (bottom) on 5 June 2014. The y-axis represents the relative size of hail and/or large rain drops.

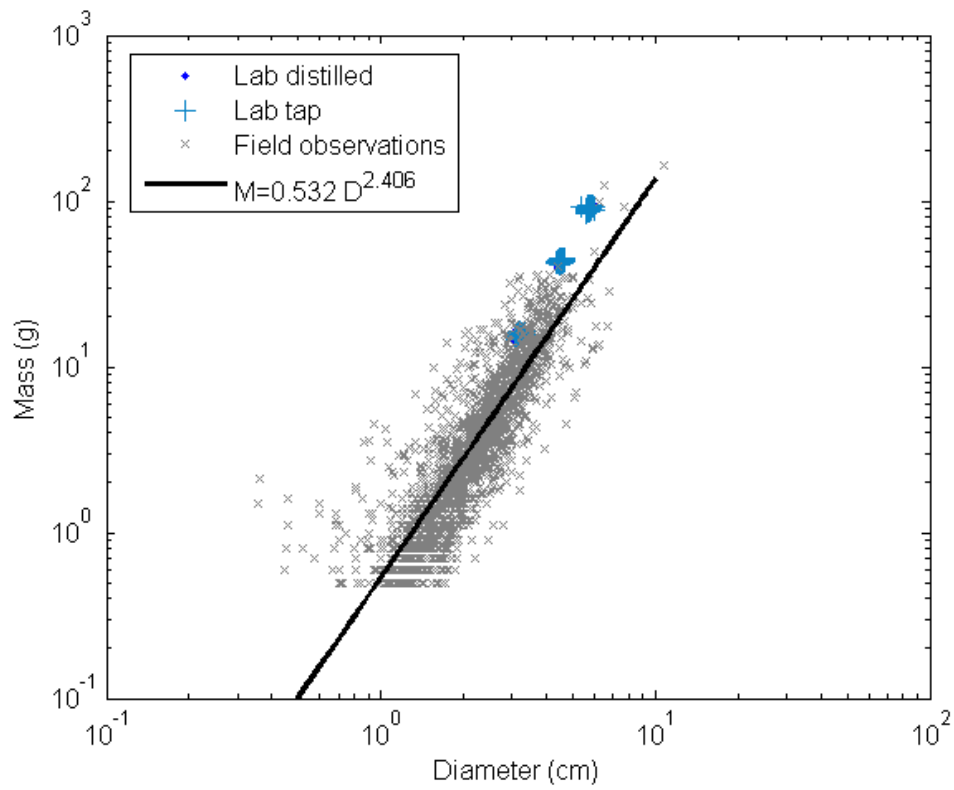


Figure 7. Hailstone mass as a function of major diameter for laboratory measurements and field observations. Also shown is the power-law fitted curve for the field observations. Power law curves for pure ice spheres of densities 0.9 and 0.2 g cm<sup>-3</sup> are provided in the companion paper (Giammanco et al. 2014).

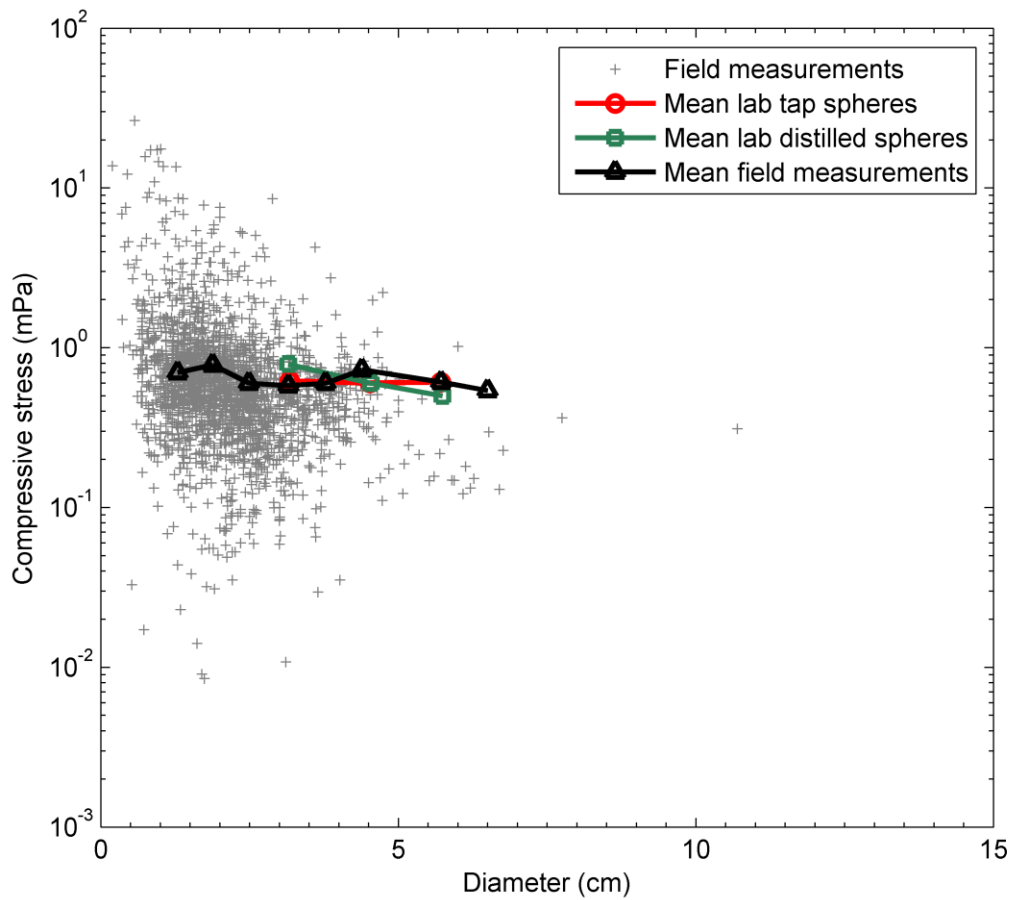


Figure 8. Compressive stress shown as a function of diameter for 2012-2014 field observations (gray), and mean values binned by diameter for field observations (black), laboratory tap water ice spheres (red), and laboratory distilled water ice spheres (green).